A Model of the Thermodynamic Structure of the Trade-Wind Boundary Layer: Part I. Theoretical Formulation and Sensitivity Tests

BRUCE A. ALBRECHT

Department of Meteorology, The Pennsylvania State University, University Park 16802

ALAN K. BETTS, WAYNE H. SCHUBERT AND STEPHEN K. COX

Department of Atmospheric Science, Colorado State University, Ft. Collins 80523

(Manuscript received 10 April 1978, in final form 5 September 1978)

ABSTRACT

A numerical model which predicts the time variation of the thermodynamic structure of the trade-wind boundary layer is developed. Horizontally homogeneous conditions are assumed and the large-scale divergence, sea surface temperature and surface wind speed are specified externally. The model predicts the average value of mixing ratio and moist static energy in the subcloud and cloud layer and the slopes of these quantities in the cloud layer; the model also predicts the height of the transition layer (the layer which defines the boundary between the cloud and subcloud layer) and the height of the trade inversion. Subcloud layer convective fluxes are specified by using the bulk aerodynamic method for specifying the surface fluxes and a mixed-layer parameterization of the fluxes at the top of the subcloud layer. The moist convective processes are parameterized in terms of a mass flux which varies linearly with height and a cloud-environment difference in thermodynamic quantities which also varies linearly with height. Radiative fluxes are parameterized in terms of a specified cloud cover and vertically averaged boundary-layer heating.

The steady-state model solutions are shown to be relatively insensitive to the specification of closure parameters. The thermodynamic structure below the inversion is shown to be sensitive to the specification of surface wind speed, sea surface temperature, radiative heating and cloud cover. The height of the inversion is shown to be sensitive to these parameters and the large-scale divergence.

1. Introduction

The trade winds are one of the most extensive and persistent features of the earth's atmosphere. A characteristic vertical structure of temperature and moisture is associated with the trades (e.g., Bunker *et al.*, 1949; Malkus, 1958; Augstein *et al.*, 1974). This structure consists of a subcloud layer where dry static energy (c_pT+gz) and water vapor mixing ratio tend to be constant with height and a cloud layer where dry static energy increases slightly with height and mixing ratio decreases with height. The upper boundary of this structure is defined by the trade inversion where dry static energy increases sharply with height and mixing ratio decreases sharply with height. The cloud layer is typically characterized by the presence of numerous shallow clouds whose tops penetrate into the trade inversion.

A considerable amount of effort has been devoted to increasing our understanding of what processes are important in maintaining the characteristic temperature and moisture structure of the trades. The investigations of Riehl *et al.* (1951), Riehl and Malkus (1957) and Malkus (1958) first suggested the importance of dry and moist convective processes in maintaining this characteristic structure. Betts (1973) theorized that the cooling and moistening due to cumulus convection maintained the inversion against the warming and drying effect of the large-scale subsidence.

The 1969 Atlantic Trade-Wind Experiment (ATEX) and the 1969 Barbados Oceanographic and Meteorological Experiment (BOMEX) provided data sets which were used to evaluate the magnitude of the convective transports in undisturbed conditions (Augstein *et al.*, 1973; Holland and Rasmussen, 1973; Nitta and Esbensen, 1974). Cumulus parameterization schemes were used to interpret the BOMEX fluxes in terms of moistening and cooling due to detrainment and warming and drying due to cumulus-induced subsidence (Betts, 1975; Nitta, 1975; Esbensen, 1976). Other studies concentrated on defining the interaction of the cloud and subcloud layer convective processes (Sarachik, 1974; Ogura and Cho, 1974; Esbensen, 1975; Betts, 1976a). Direct aircraft measurements have also been used to define the convective fluxes in the undisturbed boundary layer and to define the role of moist convective elements in contributing to these fluxes (LeMone and Pennell, 1976).

In studying the undisturbed boundary layer, observa-

0022-4928/79/010073-17$08.25

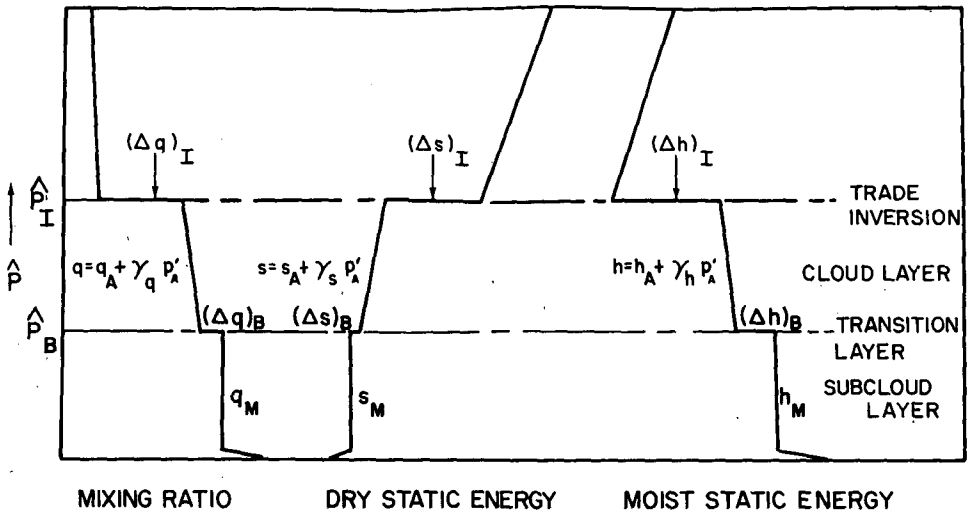

FIG. 1. Idealized boundary-layer structure assumed for the model. The symbol p_a is defined as $p_a=\hat{p}-(\hat{p}_I+\hat{p}_B)/2$.

tional and diagnostic theoretical studies have been useful in defining the vertical thermodynamic structure, determining the convective fluxes corresponding to that structure, and diagnostically testing various cumulus parameterization schemes. It is difficult, however, to use these studies to quantitatively evaluate how various parameters (such as sea surface temperature, large-scale subsidence and surface wind speed) affect the boundary-layer structure and the related fluxes. Such an evaluation is possible with a predictive model since it is relatively easy to perform controlled experiments with such a model. Although several cumulus parameterization schemes have been proposed (Ooyama, 1971; Betts, 1973; Kuo, 1965, 1974; Arakawa and Schubert, 1974; Fraedrich, 1973, 1976; Esbensen, 1976) a model which satisfactorily predicts the thermodynamic structure of the trades has not been developed.

Betts (1973) developed a model which described the undisturbed boundary layer in terms of a simple layered structure consisting of a subcloud layer, a cloud layer and an inversion layer. Solutions from this model, however, have not been completed. Ogura *et al.* (1977) described a simple layered model of the trade inversion which gives the steady-state thermodynamic structure provided that the surface fluxes and the large-scale divergence are specified externally. Results obtained from sensitivity tests made with this model, however, indicate that the applicability of the model may be limited (Ogura *et al.*, 1977). Sommeria (1976) circumvented the parameterization problem by incorporating moisture into a three-dimensional turbulence model developed by Deardorff (1972) in order to simulate the structure of the trade-wind boundary layer. Although this model gives the mean structure, as well as detailed information on the structure of the turbulence, a 5 h simulation requires ~30 h of CDC 7600 computer time.

In this paper a time-dependent model which predicts the structure of the trade-wind boundary layer is developed. The basic structure of the model is similar to the layered structure assumed by Betts (1973); convective and radiative processes in the model are parameterized using simple schemes. Horizontally homogeneous conditions are assumed and the large-scale divergence, sea-surface temperature and surface wind speed are specified externally. The model is tested by determining the sensitivity of the model to the specification of various external parameters. Further investigation of the model solutions are described in Albrecht (1979, hereafter referred to as Part II).

2. Predictive equations

The boundary-layer structure assumed for the model developed in this paper is shown in Fig. 1. The quantities shown in this figure are water vapor mixing ratio q, dry static energy s, and moist static energy h, where

$$s=c_pT+gz, \tag{1}$$

$$h=c_pT+gz+Lq. \tag{2}$$

The symbol c_p in (1) and (2) is the specific heat of air at constant pressure, T absolute temperature, g the acceleration of gravity and z the height above the surface. The symbol L in (2) represents the latent heat of vaporization. The model is formally developed in terms of h and q, although s is easily obtained since $s=h-Lq$. The vertical coordinate used in the model is $\hat{p}=p_0-p$, where p is pressure and p_0 is surface pressure. The idealized structure shown in Fig. 1 closely resembles the structure that is observed in the trade winds (Augstein *et al.*, 1974). It consists of a subcloud layer where moist static energy h_M and mixing ratio q_M are constant with height. The top of the subcloud layer is defined by an infinitesimally thin transition layer at $\hat{p}=\hat{p}_B$; the

jump in h and q at the transition layer are given as $(\Delta h)_B = h(\hat{p}_{B+}) - h_M$ and $(\Delta q)_B = q(\hat{p}_{B+}) - q_M$.

Mixing ratio and moist static energy in the cloud layer are assumed to vary linearly with height and are represented as

$$h = h_A + \gamma_h(\hat{p} - \hat{p}_A), \tag{3}$$

$$q = q_A + \gamma_q(\hat{p} - \hat{p}_A), \tag{4}$$

where h_A and q_A represent mean values for the layer, γ_h and γ_q are the slopes of moist static energy and mixing ratio in the cloud layer, and $\hat{p}_A$ is the pressure at the midpoint of the layer. The inversion layer which caps the cloud layer is assumed to be infinitesimally thin and is located at $\hat{p} = \hat{p}_I$. The jumps in h and q across the inversion are designated as $(\Delta h)_I = h(\hat{p}_{I+}) - h(\hat{p}_{I-})$ and $(\Delta q)_I = q(\hat{p}_{I+}) - q(\hat{p}_{I-})$. The structure above the inversion is assumed to be specified or given by a separate model formulation, so that $h(\hat{p}_{I+})$ and $q(\hat{p}_{I+})$ are known quantities in the model. A simplified structure similar to that described above was considered by Betts (1973), although he considered an inversion of finite thickness.

The time variation of the structure shown in Fig. 1 may be formulated mathematically by considering the area-averaged budget equations for h and q. Detailed derivations of the equations presented in this section are given in Albrecht (1977, hereafter referred to as A77). Horizontally homogeneous conditions are assumed so that horizontal advection terms will not be considered in the budget equations. Since h and q are assumed to be constant with pressure in the mixed layer, the budget equations for h_M and q_M may be written as

$$\frac{\partial h_M}{\partial t} = -g\frac{[(F_h)_{B-} - (F_h)_0]}{\hat{p}_B} - g\frac{[(F_R)_B - (F_R)_0]}{\hat{p}_B}, \tag{5}$$

$$\frac{\partial q_M}{\partial t} = -g\frac{[(F_q)_{B-} - (F_q)_0]}{\hat{p}_B}, \tag{6}$$

where F_h is the convective flux of h, F_q the convective flux of q, and F_R the net radiative flux. The subscript 0 refers to fluxes at the surface and the subscript $B-$ refers to fluxes at the top of the subcloud layer but just below the transition layer. The radiative fluxes are assumed to have no flux discontinuity at cloud base so that there is no distinction between the radiative flux just below and just above the transition layer. Physically, (5) and (6) are easily interpreted since they simply relate the time variation of subcloud layer moist static energy and mixing ratio to the divergence of the fluxes in the layer. Similar equations describing the time variation of mixed layer quantities have been discussed by Lilly (1968), Betts (1973), Ogura and Cho (1974), Arakawa and Schubert (1974) and others.

In the cloud layer the equation predicting the mean value of h is

$$\frac{\partial h_A}{\partial t} = \gamma_h\left(\frac{\partial \hat{p}_A}{\partial t} - \hat{\omega}_A\right) - g\frac{[(F_h)_{I-} - (F_h)_{B+}]}{\delta\hat{p}} - g\frac{[(F_R)_{I-} - (F_R)_B]}{\delta\hat{p}}, \tag{7}$$

where $\delta\hat{p} = \hat{p}_I - \hat{p}_B$ and $\hat{\omega}_A$ is the average large-scale vertical velocity in the cloud layer, where $\hat{\omega} \equiv d\hat{p}/dt$. The time variation of $\hat{p}_A$ which appears in (7) will be defined below.

The subgrid-scale fluxes in the cloud layer are due to moist cumulus convection. Consequently, the appropriate conservative moisture quantity in the cloud layer is total water $q+l$, where l is the liquid water mixing ratio. Betts (1975) suggested that the time variation of the mean liquid water content in the trade-wind boundary layer may be neglected. Furthermore, conventional observational techniques measure q not the total water $q+l$. Consequently, for the purpose of initializing the model and comparing model results to observations it is useful to assume that $q \approx q+l$. For typical trade cumulus situations this approximation should result in no more than a 5% overestimate of q. With these assumptions the equation describing the time variation of the average mixing ratio in the cloud layer may be written

$$\frac{\partial q_A}{\partial t} = \gamma_q\left(\frac{\partial \hat{p}_A}{\partial t} - \hat{\omega}_A\right) - g\frac{[(F_{q+l})_{I-} - (F_{q+l})_{B+}]}{\delta\hat{p}}. \tag{8}$$

Note that the convective fluxes in (8) are the fluxes of total water. It should also be noted that if a more exact interpretation of the results is desired, the mixing ratio q that appears throughout this paper should be interpreted as $q+l$. Likewise, the dry static energy s should be interpreted as $s - Ll$. Eqs. (7) and (8) relate the mean values of h and q in the cloud layer to the divergence of the fluxes in the layer. Unlike the mixed layer, these mean values may also be altered by the large-scale vertical motion ($\gamma_h\hat{\omega}_A$ and $\gamma_q\hat{\omega}_A$ terms) and changes in the mean height of the layer [$\gamma_h(\partial\hat{p}_A/\partial t)$ and $\gamma_q(\partial\hat{p}_A/\partial t)$ terms].

The analysis is simplified by assuming that the large-scale vertical velocity is linear with pressure so that

$$\hat{\omega} = -D\hat{p}, \tag{9}$$

where D is the vertically averaged large-scale divergence. Using (9), $\hat{\omega}_A$ which appears in (7) and (8) simply becomes

$$\hat{\omega}_A = -D\hat{p}_A. \tag{10}$$

Budget equations may also be used to determine how the slopes of h and q in the cloud layer vary with time.

These equations may be written

$$\frac{\partial \gamma_h}{\partial t}=D\gamma_h-4g\frac{[(F_h)_{I-}-2(F_h)_A+(F_h)_{B+}]}{\delta\hat{p}^2}-4g\frac{[(F_R)_{I-}-2(F_R)_A+(F_R)_{B+}]}{\delta\hat{p}^2}, \quad (11)$$

$$\frac{\partial \gamma_q}{\partial t}=D\gamma_q-4g\frac{[(F_{q+l})_{I-}-2(F_{q+l})_A+(F_{q+l})_{B+}]}{\delta\hat{p}^2}, \quad (12)$$

where the subscript A refers to fluxes at the midpoint of the cloud layer. Eqs. (11) and (12) simply relate the time variations in the slopes to the divergence and to flux terms which are equivalent to the second derivatives of the fluxes.

For the infinitesimally thin transition layer the budget equations become

$$(\Delta h)_B\left(\frac{\partial \hat{p}_B}{\partial t}-\hat{\omega}_B\right)=g[(F_h)_{B+}-(F_h)_{B-}], \quad (13)$$

$$(\Delta q)_B\left(\frac{\partial \hat{p}_B}{\partial t}-\hat{\omega}_B\right)=g[(F_{q+l})_{B+}-(F_q)_{B-}], \quad (14)$$

where $\hat{\omega}_B$ is the vertical velocity at the top of the subcloud layer. The discontinuity in the radiative fluxes at cloud base has been assumed to be zero. For the inversion layer the budget equations become

$$(\Delta h)_I\left(\frac{\partial \hat{p}_I}{\partial t}-\hat{\omega}_I\right)=-g(F_h)_{I-}+g[(F_R)_{I+}-(F_R)_{I-}], \quad (15)$$

$$(\Delta q)_I\left(\frac{\partial \hat{p}_I}{\partial t}-\hat{\omega}_I\right)=-g(F_{q+l})_{I-}, \quad (16)$$

where the convective fluxes at the top of the inversion have been assumed to be zero. Eqs. (13)–(16) simply relate the time variation of the height of the layer relative to the mean vertical velocity and the flux divergence across the layer. A discontinuity in the radiative fluxes is included in (15) to account for the cloud-top cooling of clouds penetrating the inversion. A similar discontinuity in the radiative fluxes is considered in models of stratocumulus convection (Lilly, 1968; Schubert, 1976). Eqs. (13)–(16) may be used to predict the height of the subcloud layer and the height of the trade inversion. Using these expressions, the $\partial\hat{p}_A/\partial t$ term which appears in (7) and (8) may be eliminated since $\hat{p}_A=(\hat{p}_B+\hat{p}_I)/2$.

The equations derived in this section formalize the time variation of the boundary layer structure in terms of the large-scale divergence and the convective and radiative fluxes. The divergence D is specified as an external parameter. Consequently, if the convective and radiative fluxes are expressed in terms of the large-scale thermodynamic structure, the equations derived in this section will represent a closed set of equations which can be used to predict the boundary-layer structure. Sections 3 and 4 are devoted to the parameterization of the convective and radiative fluxes. The numerical integration of the equations derived in this section will be considered in Section 5.

3. Parameterization of convective fluxes

The bulk aerodynamic method is used to specify the surface fluxes as

$$(F_h)_0=\rho_0C_TV_0(s_0-s_M)+\rho_0C_qV_0L(q_0-q_M), \quad (17)$$

$$(F_q)_0=\rho_0C_qV_0(q_0-q_M), \quad (18)$$

where ρ_0 is the density of air near the surface, V_0 the wind speed at a height of 10 m, and $s_0=c_pT_0$, where T_0 is the sea surface temperature and q_0 the saturation mixing ratio of air at the sea surface temperature. The coefficients C_q and C_T in (17) and (18) are the bulk aerodynamic coefficients for moisture and sensible heat transfer defined at the top of the surface layer.

In the ATEX data the surface layer extends to 100–150 m so that the differences (q_0-q_M) and (s_0-s_M) will be larger than the corresponding air-sea differences at 10 m height. Consequently, the transfer coefficients obtained from measurements made at 10 m should be appropriately reduced when the surface fluxes are defined from data at a higher level (Fissel *et al.*, 1977). For simplicity it is assumed that $C_T=C_q=1.15\times10^{-3}$ which represents a reduction of approximately 10% in the coefficients obtained by Friehe and Schmitt (1976) from various data sets.

The fluxes at the top of the mixed layer are specified by assuming that

$$(F_{sv})_{B-}=-k(F_{sv})_0, \quad (19)$$

where $(F_{sv})_{B-}$ is the flux of virtual dry static energy s_v just below cloud base; $(F_{sv})_0$ is the surface flux of virtual dry static energy at the surface and k is a constant. Similar closure schemes have been used in treatments of the dry mixed layer and the subcloud layer (e.g., Lilly, 1968; Betts, 1973; Tennekes, 1973).

Since the virtual fluxes of dry static energy in the subcloud layer may be defined as

$$F_{sv}=F_h-(1-\delta\epsilon)LF_q, \quad (20)$$

where $\delta=0.608$ and $\epsilon=c_p\bar{T}/L$, Eq. (19) represents one equation for the two unknowns $(F_h)_{B-}$ and $(F_q)_{B-}$. A second equation for these variables is obtained by assuming that the discontinuities in h and q at the transition layer are maintained at the same height. This assumption allows (13) and (14) to be combined to give the consistency relationship

$$\frac{(F_q)_{B-}}{(\Delta q)_B}-\frac{(F_h)_{B-}}{(\Delta h)_B}=\frac{(F_{q+l})_{B+}}{(\Delta q)_B}-\frac{(F_h)_{B+}}{(\Delta h)_B}. \quad (21)$$

The cloud-layer fluxes $(F_h)_{B+}$ and $(F_{q+l})_{B+}$ which appear in (21) are defined in the following section. It will be shown below that these definitions allow (21) to be reduced to

$$\frac{(F_q)_{B-}}{(\Delta q)_B}=\frac{(F_h)_{B-}}{(\Delta h)_B}. \tag{22}$$

Eqs. (19), (20) and (22) may be combined to give the fluxes at the top of the subcloud layer as

$$(F_h)_{B-}=-\frac{k(\Delta h)_B}{(\Delta s_v)_B}(F_{sv})_0, \tag{23}$$

$$(F_q)_{B-}=-\frac{k(\Delta q)_B}{(\Delta s_v)_B}(F_{sv})_0. \tag{24}$$

The basic formulation of the convective fluxes in the cloud layer is similar to that suggested by Ooyama (1971), Yanai *et al.* (1973) and Betts (1975). The assumption in this scheme is that the convective fluxes may be separated into a characteristic mass flux associated with the convective elements, and the difference between the thermodynamic characteristics of the cloud and the average characteristics of the cloud layer. Using this formulation, the flux of h and $q+l$ due to convective elements may be written

$$F_h=\omega^*(h_c-h)/g, \tag{25}$$

$$F_{q+l}=\omega^*(q_c+l_c-q)/g, \tag{26}$$

where h_c, q_c and l_c refer to in-cloud values and h and q, as was assumed previously, refer to values averaged over some horizontal area which is much larger than the fractional area covered by an individual cloud. It will be convenient to refer to the quantities (h_c-h) and (q_c+l_c-q) as cloud-environment differences. The symbol ω^* represents the convective mass flux which is specified to be the product of the fractional area σ covered by active updrafts and a characteristic updraft velocity. In the derivation of (25) and (26) it is assumed that $\sigma\ll 1$.

In the parameterization scheme presented below ω^* is defined to represent the mass flux of all active clouds averaged over the active lifetime of these clouds. The cloud-environment differences in (25) and (26) are also defined as an average over the lifetime of these clouds. With these definitions the convective fluxes may be formulated without considering a spectrum of clouds such as that employed by Arakawa and Schubert (1974). Betts (1975) used BOMEX data to demonstrate the validity of using such a transient cloud model for shallow nonprecipitating convection.

The parameterization of the convective fluxes in the cloud layer is somewhat simplified since the profiles of h and q are assumed to be linear with pressure in the cloud layer. To be consistent with the assumed structure, the fluxes in the cloud layer must vary quadratically with pressure. For simplicity, it is assumed that the mass flux and the cloud-environment differences that appear in (25) and (26) vary linearly with pressure so that

$$gF_h=-\omega_B^*(1+\mu p')(\Delta h)_{CB}(1+\lambda_h p'), \tag{27}$$

$$gF_{q+l}=-\omega_B^*(1+\mu p')(\Delta q)_{CB}(1+\lambda_q p'), \tag{28}$$

where $p'\equiv\hat{p}-\hat{p}_B$, $-(\Delta h)_{CB}$ and $-(\Delta q)_{CB}$ are the cloud-environment differences at cloud base, and ω_B^* is the mass flux at cloud base. The parameters μ, λ_h and λ_q give the vertical distribution of mass flux and cloud-environment differences. The remainder of this section will be devoted to formulating expressions for $(\Delta h)_{CB}$, $(\Delta q)_{CB}$, ω_B^*, λ_h, λ_q and μ.

The cloud-environment differences at cloud base are specified by assuming that the air rising into clouds has properties similar to that of the subcloud layer. Observations indicate, however, that air near the base of clouds is slightly more moist and possibly cooler than the surrounding subcloud layer (LeMone and Pennell, 1976). In the aircraft measurements made by LeMone and Pennell, for example, the air just beneath clouds was typically more moist by $\sim$0.4 g kg^{-1} and cooler by $\sim$0.1°C than the surrounding subcloud layer. If the deviations of h_c and q_c at cloud base from the subcloud layer values are defined as δh and δq, the cloud-environment differences at cloud base may be written

$$-(\Delta h)_{CB}=-(\Delta h)_B+\delta h, \tag{29}$$

$$-(\Delta q)_{CB}=-(\Delta q)_B+\delta q. \tag{30}$$

No attempt is made here to theoretically predict δq and δh. For simplicity it is assumed that

$$\frac{\delta q}{(\Delta q)_B}=\frac{\delta h}{(\Delta h)_B}, \tag{31}$$

where δq is specified as a constant. As noted above, Eqs. (27)–(31) allows (21) to be reduced to (22).

The cloud-base mass flux ω_B^* may be determined by defining cloud base to be at the top of the mixed layer. This assumption is made by Betts (1973) and Stull (1976a) and is used here to define the fluxes of F_h and F_{q+l} at cloud base from which ω_B^* may be determined. If cloud parcels are assumed to become saturated at the top of the mixed layer, then the definition s_M, q_M and $\hat{p}_B$ are related. This relationship may be written as

$$\tilde{\omega}_B\equiv\frac{\partial\hat{p}_B}{\partial t}=f_1\frac{\partial s_M}{\partial t}-f_2\frac{\partial q_M}{\partial t}$$

or

$$\tilde{\omega}_B=f_1\frac{\partial h_M}{\partial t}-(Lf_1+f_2)\frac{\partial q_M}{\partial t}, \tag{32}$$

where the functions f_1 and f_2 are positive and depend on the boundary-layer structure. Eqs. (5) and (6) may be used to eliminate the time derivatives of h_M and q_M from (32) so that $\tilde{\omega}_B$ can be evaluated in terms of the

mixed-layer fluxes. The functions f_1 and f_2 are defined in the Appendix.

Eqs. (13) and (14) may be used to evaluate the fluxes just above the transition layer as

$$(F_h)_{B+}=(F_h)_{B-}+(\Delta h)_B(\tilde{\omega}_B-\hat{\omega}_B)/g, \tag{33}$$

$$(F_{q+l})_{B+}=(F_q)_{B-}+(\Delta q)_B(\tilde{\omega}_B-\hat{\omega}_B)/g. \tag{34}$$

Eqs. (33) and (34) simply give the flux discontinuity across the transition layer that is required to maintain the height of the transition layer at cloud base. Although the fluxes $(F_h)_{B+}$ and $(F_{q+l})_{B+}$ are the parameters which are needed to specify the fluxes given in the predictive equations, it is useful to note that the cloud-base mass flux may be determined from (27) and (28) as

$$\overset{*}{\omega}_B=-g\frac{(F_{q+l})_{B+}}{(\Delta q)_{CB}}=-g\frac{(F_h)_{B+}}{(\Delta h)_{CB}}. \tag{35}$$

The cloud-environment difference in thermodynamic variables above cloud base which is represented in (27) and (28) may be formalized by considering the entrainment relationships

$$\frac{\partial(q_c+l_c)}{\partial\hat{p}}=-\frac{E}{\delta\hat{p}}(q_c+l_c-q), \tag{36}$$

$$\frac{\partial h_c}{\partial\hat{p}}=-\frac{E}{\delta\hat{p}}(h_c-h), \tag{37}$$

where E is an entrainment parameter assumed to be constant with pressure. Similar entrainment relationships have been used by Ooyama (1971), Yanai *et al.* (1973), Arakawa and Schubert (1974) and Betts (1973). Since q and h are linear functions of pressure, Eqs. (36) and (37) are easily integrated to obtain exact solutions for the cloud-environment differences. These exact solutions are approximated as linear functions such that λ_h and λ_q in (27) and (28) are defined as

$$\lambda_h=\left[\frac{\gamma_h}{(\Delta h)_{CB}}-\frac{E}{\delta\hat{p}}\right]\left(1-\frac{E}{3}\right), \tag{38}$$

$$\lambda_q=\left[\frac{\gamma_q}{(\Delta q)_{CB}}-\frac{E}{\delta\hat{p}}\right]\left(1-\frac{E}{3}\right). \tag{39}$$

A derivation of the λ_h and λ_q parameters is given in A77. For realistically possible values of γ_h, γ_q, $(\Delta h)_{CB}$ and $(\Delta q)_{CB}$, the linear cloud-environment differences given by using (38) and (39) differ from the exact solutions by less than 10% at all levels for $E\leqslant 0.60$ and less than 3% for $E\leqslant 0.20$.

The entrainment parameter E is determined by assuming that the cloud-environment difference in virtual temperature averaged over the cloud-layer depth is a constant. This is approximately equivalent to assuming that the buoyancy force averaged over the depth of the cloud layer is a constant. Mathematically this constraint may be written as

$$(1/c_p\delta\hat{p})\int_0^{\delta\hat{p}}(s_{vc}-s_v)d\hat{p}'=\Delta T_0, \tag{40}$$

where ΔT_0 is a positive constant, s_{vc} the virtual dry static energy of the cloud parcels and s_v the virtual dry static energy of the environment. The rationale behind the constraint given by (40) is that the parameterized clouds in the model must be maintained by buoyancy forces. Simply assuming a constant value of E would not insure that the clouds considered were positively buoyant. The constraint given by (40) also insures that cloud buoyancy does not become unrealistically large.

Constraints similar to (40) have been used in the parameterization theories proposed by Betts (1973) and Arakawa and Schubert (1974). The way in which they applied this constraint, however, is different than that being proposed here. In the model proposed by Betts (1973) an inversion of finite depth was considered. The negative buoyancy of cloud parcels in the inversion layer was constrained to be a specified fraction of the positive buoyancy generated in the cloud layer. In this formulation however, the entrainment parameter E was specified and the stratification of the large-scale environment was altered to satisfy the buoyancy constraint and a liquid water constraint. In the Arakawa and Schubert (1974) parameterization scheme a cloud work function $A(\lambda)$ for a particular cloud type λ was defined as the vertical integral of the buoyancy force weighted by the normalized mass flux distribution. The quasi-equilibrium assumption used to close the Arakawa and Schubert parameterization was that $\partial A(\lambda)/\partial t=0$. This expression is basically equivalent to (40) although the buoyancy force is not weighted by the mass flux distribution. In the Arakawa and Schubert treatment, however, the cloud type is synonymous with a specific entrainment rate and the quasi-equilibrium assumption is applied to determine the cloud-base mass flux for each cloud type.

In the parameterization presented here, Eq. (40) is used to determine the entrainment factor E. The interesting aspect of this parameterization is that it tends to maintain a convectively active cloud layer in spite of the stabilizing effect of the large-scale subsidence. Qualitatively this may be demonstrated by noting that if the cloud layer becomes more stable s_v would increase more rapidly with height. Consequently, s_{vc} would also have to increase more rapidly with height in order to satisfy (40). This greater increase of s_{vc} may be accomplished by decreasing E. As entrainment decreases, however, it may be shown that the effect of the convection in the model is to decrease the cloud-layer stability (A77). Thus a balance may be achieved between the tendency of subsidence to stabilize the layer and the tendency of nonprecipitating convection to destabilize the layer. A quantitative expression for

the entrainment factor E derived from (40) is given in the Appendix.

The factor μ which defines the vertical distribution of mass flux is obtained by considering a transient cloud model such as that suggested by Betts (1975) and Fraedrich (1976). In the transient cloud model the important concept is that the cloud properties are defined over the active lifetime of the cloud. To formalize this concept a very simple cloud model is considered. In this model the cloud has a uniform updraft velocity during the active lifetime of the cloud. Only one cloud type is considered so that all clouds are assumed to reach the trade inversion during their lifetime. An entrainment relationship is used to describe the variation with height of the area covered by active updrafts. Using this very simple model, the convective mass flux in the cloud layer may be approximated as

$$\omega^* = \omega_B^*(1+\mu p'), \tag{41}$$

where

$$\mu = \begin{cases} \dfrac{E}{\delta\hat{p}} - \dfrac{\sigma_0}{\omega_B^* \tau_c}(1+\frac{2}{3}E), & p' \leqslant \delta\hat{p} \\ -1/p', & p' > \delta\hat{p}. \end{cases} \tag{42}$$

The symbol σ_0 in (42) is the fractional area covered by active updrafts at cloud base and τ_c is the lifetime of the clouds. A complete derivation of (42) is given in A77.

As demonstrated by Betts (1975) using a similar derivation, the term

$$\frac{\sigma_0}{\omega_B^* \tau_c}(1+\tfrac{2}{3}E) \tag{43}$$

in (42) represents a decrease in mass flux with height which is equivalent to a detrainmant of cloud mass. Betts used BOMEX data to show that this term may dominate the mass flux distribution in undisturbed conditions resulting in a mass flux which decreases with height. The discontinuity in the mass flux at the inversion represents a detrainment of mass at this level due to a loss of buoyancy by the clouds. A similar detrainment process is considered by Arakawa and Schubert (1974).

The parameters τ_c and σ_0 may be difficult to evaluate from observations and may be even more difficult to obtain from theoretical arguments. It may be shown, however, (see A77) that τ_c/σ_0 corresponds to a time scale for variations in the cloud-layer stability due to convection. For simplicity the mass flux distribution given by (42) is specified by assuming that

$$\tau_a \equiv \tau_c/2\sigma_0 = \text{constant}. \tag{44}$$

This implies that as the lifetime of clouds increases, the fractional area of active updrafts also increases. The observational results given by Betts (1975) for BOMEX suggest $\tau_a \approx \frac{1}{3}$ day. For a cloud cover of active updrafts of 0.02, this τ_a corresponds to a cloud lifetime of $\sim$20 min. The sensitivity of the model results to the specification of τ_a is shown in Section 5.

Using the definitions given above for $(\Delta q)_{CB}$, $(\Delta h)_{CB}$, ω_B^*, λ_h, λ_q and μ the convective fluxes in the cloud layer may be defined by evaluating (27) and (28). The details needed for computing these convective fluxes are outlined in the Appendix.

4. Parameterization of radiative fluxes

The radiative heating in the boundary layer results from the absorption and emission of longwave radiation (in the wavelength interval 3–60 μm) and the absorption of shortwave radiation (in the wavelength interval 0.3–3.0 μm) by various atmospheric constituents. Although the heating may vary with the quantity of ozone, carbon dioxide and water vapor in the atmosphere, clouds have been clearly shown to be the principal modulators of the radiative processes (e.g., Starr, 1976). Although trade cumulus are finite clouds, the radiation processes will be defined separately for clear sky conditions and for clouds of infinite horizontal extent. The radiative heating rates will then be determined as a weighted average of heating rates obtained for clear and cloudy conditions.

Since the model described above is constrained to have a constant s in the mixed layer and a linear s in the cloud layer, the radiative processes that need to be considered are those which change the mean values of s in the cloud and subcloud layer and those which change the slope of s in the cloud layer. It is also necessary to determine the discontinuity in the radiative fluxes at the inversion in order to predict the height of the inversion. To obtain a simple scheme for parameterizing the radiative fluxes, heating rates for several representative boundary-layer structures were obtained from a detailed broadband radiative transfer calculation. These detailed calculations were then generalized to form a simple parameterization of the radiative processes.

A number of calculations were made to determine the sensitivity of clear-sky longwave heating rates to variations in the temperature, moisture and depth of the boundary layer. These calculations were made using the broadband radiative transfer model described by Cox (1973); this model includes the effect of continuum broadening. The basic temperature and moisture structure used for these calculations was similar to that observed for the ship *Planet* from 7–12 February during ATEX (Augstein *et al.*, 1974). Climatological values of carbon dioxide and ozone were assumed for the calculation.

The moisture structure was varied by altering the mean value of mixing ratio in the cloud and subcloud layer and its rate of decrease in the cloud layer. Calculations were made for boundary-layer depths of 130 and 170 mb. Although no extreme variations in the mixing ratios were considered, the boundary-layer precipitable water varied from 1.51 to 2.42 cm for

TABLE 1. Vertically averaged clear-sky longwave heating for various boundary-layer moisture structures.

Boundary layer precipitable water (cm)	Boundary-layer depth (mb)	γ_q (g kg^{-1} mb^{-1})	Longwave radiative heating (°C day^{-1})
2.06	170	0.000	−4.03
2.00	170	−0.050	−4.04
1.94	170	−0.030	−4.05
1.88	170	−0.050	−4.04
1.58	130	−0.000	−4.05
1.56	130	−0.015	−4.05
1.54	130	−0.030	−4.04
1.51	130	−0.050	−4.04
1.61	130	−0.015	−4.10
2.42	130	−0.015	−4.46

these calculations. A detailed description of the model atmospheres used for these sensitivity tests is given in A77. The longwave heating rates obtained from these calculations and averaged from the trades inversion to the ocean surface are shown in Table I. It is interesting to note that these vertically averaged heating rates vary by less than 0.5°C day^{-1} for these calculations. The heating rates calculated for different structures of cloud-layer temperature also resulted in very small variations in the vertically averaged heating rates (A77).

Although the average heating is relatively insensitive to variations in the boundary-layer temperature and moisture, the vertical distribution of heating does depend slightly on these variables. In A77 the vertical distribution of heating was parameterized in terms of the boundary-layer temperature and moisture. This parameterization scheme produced steady-state model results which did not vary significantly from the results obtained by assuming the boundary-layer heating to be uniformly distributed in the vertical. Consequently, for the results shown in this paper it is assumed that the boundary-layer clear-sky infrared heating rates are uniformly distributed in the vertical.

The longwave cooling within clouds was evaluated by considering a horizontally infinite cloud with a broadband emissivity ϵ_c within the cloud that is formulated in the exponential form suggested by Paltridge (1974). This form is given as

$$\epsilon_c(\zeta) = 1 - \exp[-a_0 w(\zeta)], \tag{45}$$

where ζ is the distance from the cloud boundary to some point within the cloud and a_0 is interpreted as a mass absorption coefficient. The parameter w in (45) is defined as

$$w = \int_0^{\zeta} \mathrm{LWC}\, dz, \tag{46}$$

where LWC is the liquid water content of the cloud. The emissivity as given by (45) is incorporated into the clear-sky radiative transfer calculation described by Cox (1973). The details of this calculation are given by Griffith and Cox (1977). A similar method is described by Feigel'son (1973).

The use of (45) in the transfer calculation requires that LWC and a_0 be specified. In the calculations discussed below a_0 is assumed to be 500 g^{-1} cm^{-2}. A linear profile of liquid water content was assumed for the transfer calculations. Calculations were made for a cloud with cloud top at 845 mb, cloud base at 930 mb and mean liquid water contents of 0.25 and 0.50 g m^{-3}. The temperature and mixing ratio were specified to be similar to that observed at the *Planet* from 7–12 February during ATEX. The net fluxes calculated for these cloud models are shown in Fig. 2; the distributions indicate that the net flux has no significant variation with liquid water content. These results show a strong cooling in the top 10 mb of the cloud layer, little radiative effect in the cloud, slight warming near cloud base and slight cooling near the surface.

The longwave heating averaged from the surface to the top of the inversion for the calculations described above are given in Table 2. The average heating obtained for a cloud with cloud base at 930 mb and cloud top at 845 mb is also shown in this table. Although the average boundary-layer cooling is relatively constant for these calculations, the important feature to note is that the longwave cooling is approximately equivalent to the clear-sky calculated cooling.

Calculations were also made to estimate the clear-sky boundary-layer heating due to the absorption of solar radiation by water vapor, carbon dioxide and ozone. A broadband irradiance calculation based on the absorptivity values given by Manabe and Möller (1961) was used for this calculation. The heating rates obtained from these calculations were nearly uniformly distributed in the vertical, while the vertically averaged boundary-layer heating was found to be insensitive to variations in moisture. The heating rate averaged over a 24 h period and averaged over the depth of the boundary layer is ~0.8° day^{-1} for these calculations.

The absorption of solar radiation by clouds in a process which has not been satisfactorily quantified. There are few direct measurements of the solar absorption by clouds and these measurements do not agree

TABLE 2. Vertically averaged longwave heating rates for various cloud models.

Average liquid water content (g m^{-3})	Cloud-top pressure (mb)	Cloud-base pressure (mb)	Longwave heating (°C day^{-1})
0.50	845	930	−4.11
0.25	845	930	−4.03
0.25	875	930	−4.59

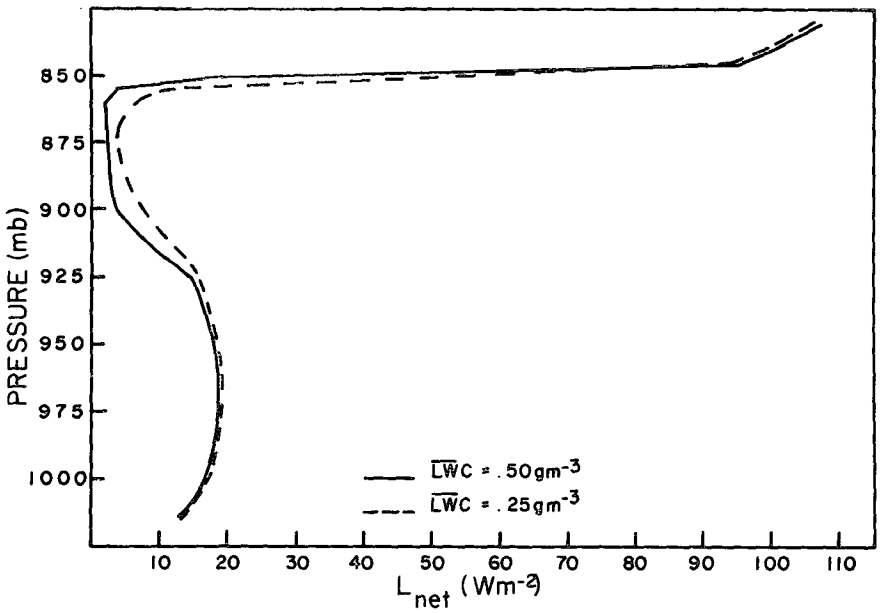

FIG. 2. The net longwave fluxes calculated for horizontally infinite clouds having mean liquid water contents of 0.50 and 0.25 g m^{-3}. Cloud base is at a pressure of 930 mb and top at 845 mb.

with theoretical calculations (Reynolds *et al.*, 1975; Liou, 1976; Twomey, 1976). For simplicity it is assumed that the solar absorption in the boundary layer is the same for both cloud and clear conditions. In the cloud case, however, this absorption occurs in a thin layer at cloud top while in the clear case it is uniformly distributed. This assumption is equivalent to assuming a cloud absorption which is not significantly different than that predicted by Liou (1976).

The results given above suggest a relatively simple scheme for the parameterization of the radiative fluxes. The longwave and shortwave heating rates averaged from the surface to $\hat{p}_I$, Q_L and Q_S respectively, are assumed to be constant and independent of the boundary-layer cloudiness, temperature or moisture distributions. In the clear regions the heating is assumed to be uniformly distributed through the depth of the boundary layer. In the cloud regions the cooling occurs in the infinitesimally thin inversion layer where the tops of mature and dying clouds are located; below the inversion layer the radiative heating is assumed to be zero.

The radiative heating for the partly cloudy conditions which are present in the trades is specified to be an average of the heating for the clear and cloudy regions weighted by the fractional amount of visible cloudiness σ_R. With these assumptions and defining the total radiative heating as $Q_R=Q_L+Q_S$, the fluxes needed for the budget equations presented in Section 2 may be defined in terms of the heating rates as

$$(F_R)_0=(F_R)_{I+}+c_p\hat{p}_I Q_R/g, \tag{47}$$

$$(F_R)_B=(F_R)_{I+}+c_p[\delta\hat{p}+\sigma_R\hat{p}_I]Q_R/g, \tag{48}$$

$$(F_R)_{I-}=(F_R)_{I+}+c_p\sigma_R\hat{p}_I Q_R/g, \tag{49}$$

$$(F_R)_A=[(F_R)_B+(F_R)_{I-}]/2. \tag{50}$$

It should be noted that the specification of $(F_R)_{I+}$ is arbitrary from the perspective of the energy budget of the various layers.

5. Sensitivity tests

In this section the convective and radiative fluxes formulated in Sections 3 and 4 will be combined with the predictive equations discussed in Section 2. The resulting equations are integrated numerically to determine the sensitivity of the model results to various specified parameters. A summary of the model unknowns and specified parameters is given in Table 3. The computational procedure for obtaining numerical results is outlined in the Appendix.

TABLE 3. A summary of model unknowns, specified physical parameters and specified closure parameters used in the model.

Model unknowns	Specified physical parameters	Specified closure parameters
q_M, h_M, q_A, h_A	T_0	C_T
γ_q, γ_h, $\hat{p}_B$, $\hat{p}_I$	V_0	C_q
$(F_q)_0$, $(F_h)_0$, $(F_R)_0$	D	k
$(F_q)_{B-}$, $(F_h)_{B-}$, $(F_R)_B$	σ_R	δ_q
$(F_{q+l})_{B+}$, $(F_h)_{B+}$	Q_L	τ_a
$(F_{q+l})_A$, $(F_h)_A$, $(F_R)_A$	Q_S	ΔT_0
$(F_{q+l})_{I-}$, $(F_h)_{I-}$	$q(\hat{p})$	
$(F_R)_{I-}$, $(F_R)_{I+}$	$h(\hat{p})$	

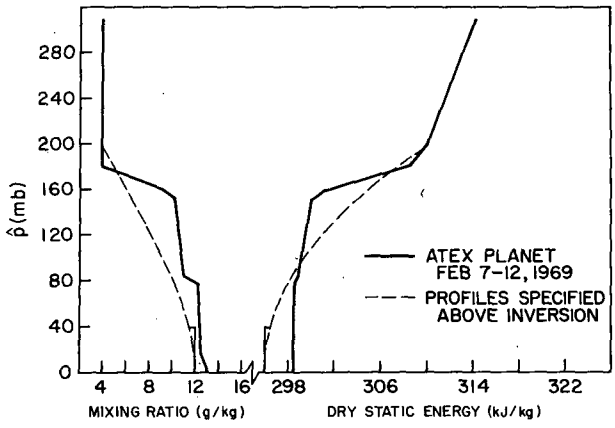

FIG. 3. Initial boundary layer structure assumed for the model and profiles of s and q assumed above the boundary layer compared with the structure observed from the *Planet* during the period 7–12 February 1969 (Augstein *et al.*, 1974).

There are two types of parameters which are specified in the model which may affect the predicted structure. Some parameters such as ΔT_0 and τ_a result from assumptions used to parameterize the convective fluxes. While some physical interpretation of these parameters is possible, it is hoped that the model results will be relatively insensitive to these parameters. Unless specifically noted otherwise, the closure parameters are specified as $\Delta T_0=0.5°C$, $\tau_a=0.333$ day, $k=0.25$ and $\delta q=0.4$ g kg^{-1}. Other specified parameters such as T_0 and V_0 are physical parameters which may vary in the real atmosphere. Values assumed for these parameters unless stated specifically otherwise are $T_0=25°C$, $V_0=7$ m s^{-1}, $D=5.7\times10^{-6}$ s^{-1}, $Q_L=-4°C$ day^{-1}, $Q_S=0.8°C$ day^{-1} and $\sigma_R=0.5$. These values were chosen to be consistent with the ATEX observations (Augstein *et al.*, 1973, 1974). Although the model is formulated in terms of q and h, the results given below will be given in terms of q and s, since the vertical profiles of q and h are generally quite similar in appearance.

The thermodynamic structure assumed above the inversion is shown in Fig. 3 with the thermodynamic structure observed from the *Planet* from 7–12 Feburary during ATEX (Augstein *et al.*, 1974). Above $\hat{p}=200$ mb the profiles assumed above the inversion are the same as those observed for the *Planet*. In the lowest 90 mb the profiles assumed above the inversion are drier and cooler than the observed profiles. From 90 to 200 mb the specified profiles are slightly warmer and drier than that observed during ATEX. The specified atmospheric structure is similar to that observed in the wake of disturbed conditions (Betts, 1976b; Seguin and Garstang, 1976).

The initial conditions assumed for the model runs, also shown in Fig. 3, consist of a mixed-layer 40 mb in depth with $q_M=12.0$ g kg^{-1} and $s_M=296.0$ kJ kg^{-1} ($h_M=325.4$ kJ kg^{-1}). The cloud layer is only considered in the model when the height of the mixed layer reaches the lifting condensation level for air having a moisture content of $q_M+\delta q$ and a dry static energy of $s_M+\delta s$. When the cloud layer first begins to form, it is assumed to have an initial depth of 5 mb and the initial values of q and s at cloud base are assumed to have the value of the specified profiles (see Fig. 3) at that level. The initial slopes of q and s are specified to be the *Planet* slopes shown in Fig. 3. It should be noted that the specification of the initial conditions in not crucial since the steady-state solutions are independent of the initial conditions provided that those conditions are physically realistic.

Steady-state results were obtained by integrating the model from the initial conditions described above until the solutions became steady. In general the predicted structure becomes nearly steady after 64 h of integration and absolutely steady after 70 h. The model fluxes for the steady-state solution demonstrate a balance between convective, radiative and large-scale processes. The steady-state model structure and fluxes obtained with the external conditions outlined above are shown in Table 4. These fluxes show that in the subcloud layer the radiative cooling is simply balanced by heating due to convection. Since precipitation and horizontal advection is ignored, the moisture flux is constant through the mixed layer. It should also be noted that the moisture flux contributes significantly to the virtual static energy flux in the subcloud layer. In the cloud layer the steady-state fluxes shown in Table 4 indicate that the radiative cooling is balanced by warming due to convective processes and large-scale subsidence. Convective moistening in the cloud layer balances the drying due to large-scale subsidence. Warming due to subsidence at the trade inversion is balanced by radiative cooling and cooling associated with the evaporation of cloud water at this level. The evaporation of cloud water also balances the drying due to subsidence at the inversion.

The fluxes shown in Table 4 also demonstrate the role of convection in maintaining the cloud layer stratification. The subsidence in the cloud layer tends to increase the slope of s and decrease the slope of q [see Eqs. (11) and (12)]. For the steady-state solution these tendencies are balanced by the curvature of the fluxes. It should be noted, however, that the cloud-layer fluxes differ only slightly from being linear with $\hat{p}$.

Several model runs were performed to evaluate the sensitivity of the steady-state model solutions to the

TABLE 4. Steady-state structure and fluxes. In the subcloud layer $F_{sl}=F_s$ and $F_{q+l}=F_q$.

$\hat{p}$ (mb)	s (kJ kg^{-1})	q (g kg^{-1})	F_{sl} (W m^{-2})	LF_{q+l} (W m^{-2})	F_R (W m^{-2})
0	299.41	13.35	1.3	156	33.5
82.7(−)	299.41	13.35	−14.3	156	49.1
82.7(+)	299.86	11.33	−12.1	132	49.1
127.2	300.57	10.15	−16.2	114	57.6
171.6(−)	301.27	8.96	−18.4	89	66.0
171.6(+)	306.37	5.35	0	0	98.6

specification of the closure parameters. The steady-state predicted for $\tau_a = \frac{1}{4}$ day and $\tau_a = \frac{1}{2}$ day are shown in Fig. 4. In the mixed layer the differences between these two models are very small. The structure predicted with an adjustment time of $\frac{1}{2}$ day results in a cloud layer which is ~ 0.5 g kg^{-1} drier and ~ 0.5°C cooler than that predicted with an adjustment time of $\frac{1}{4}$ day. The height of the inversion is approximately the same for both calculations. The slopes of q and s in the cloud layer do not vary significantly between the two calculations, although the jump in q at cloud base is somewhat sensitive to the specification of this parameter. The effect of increasing the adjustment time is equivalent to allowing the atmosphere to dry and warm slightly more due to the large-scale subsidence field.

The model results for $\Delta T_0 = 0.5$ and $\Delta T_0 = 0.0$°C are shown in Fig. 5. The principal effect of altering this parameter is to alter the slopes of q and s in the cloud layer. The larger ΔT_0 results in the layer becoming slightly more unstable. It is interesting to note that the results obtained with $\Delta T_0 = 0.0$°C more closely resemble those obtained with $\tau_a = \frac{1}{2}$ day. This suggests the possibility that these closure parameters may not be independent of each other. The results presented here, however, indicate that the steady-state solutions are not extremely sensitive to the specification of either τ_a or ΔT_0.

Model calculations were also made to determine the specification of k and δq. The structure predicted for $k = 0.40$ and $k = 0.10$ are shown in Fig. 6. Since typical values assumed for k range from 0.2 to 0.3 (Stull, 1976b), the sensitivity of the model results to this parameter is quite small indicating that its specification may not be crucial to the steady-state results. The predicted structure during the initial growth of the boundary layer is also slightly sensitive to the specification of k. These results are consistent with the mixed layer results obtained by Zeman and Tennekes (1977) for convective conditions. The structure for $\delta q = 0.0$ and $\delta q = 0.4$ g kg^{-1} is shown in Fig. 7. The specification of this parameter does result in slight differences in the

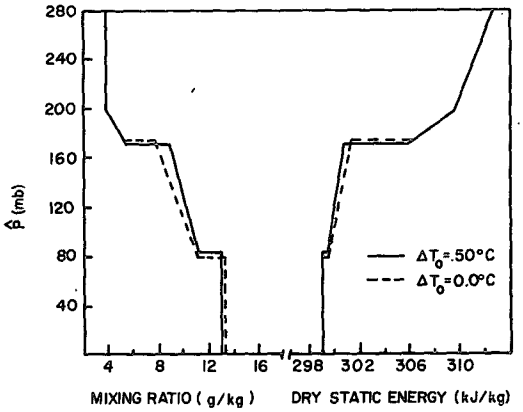

FIG. 5. As in Fig. 4 except for ΔT_0 of 0.5 and 0.0°C.

mixed-layer height and thermodynamic variables. In many modeling situations it appears that assuming clouds to have mixed-layer properties may be acceptable. It is interesting to note, however, that δT, which is derived from the model results, is ~ 0.1°C, in good agreement with the LeMone and Pennell (1976) measurements discussed previously.

The sensitivity of the model-predicted structure to physical parameters will be demonstrated in the remainder of this section. The model steady-state solutions are shown in Fig. 8 for various divergence values. The principal differences between the boundary-layer structure obtained with various divergence values is the height of the inversion. When the divergence is increased from 4×10^{-6} s^{-1} to 6×10^{-6} s^{-1}, the height of the inversion decreases by ~ 25 mb. As the divergence is increased to 8×10^{-6} s^{-1} the height of the inversion only decreases by ~ 15 mb.

The sensitivity of the inversion height to variations in the divergence is qualitatively reasonable, since for near steady-state conditions there is a balance between drying due to large-scale subsidence and moistening due to moist convection. In the dry static energy profile there is a balance between the radiative and convective cooling at the trade inversion and the

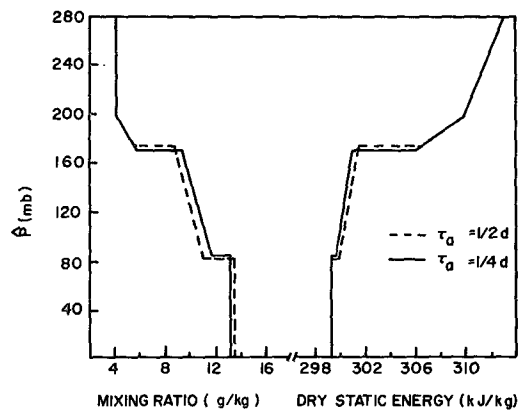

FIG. 4. Steady-state model structure for τ_a of $\frac{1}{4}$ and $\frac{1}{2}$ day.

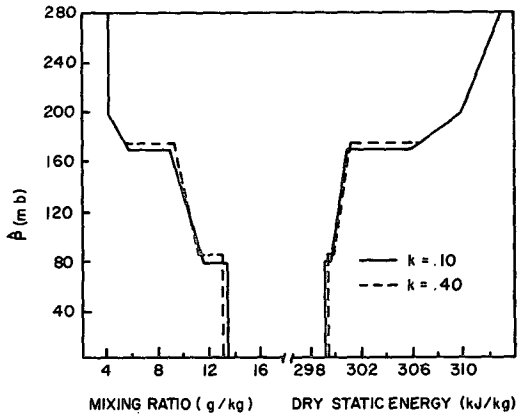

FIG. 6. As in Fig. 4 except for $k = 0.1$ and $k = 0.4$.

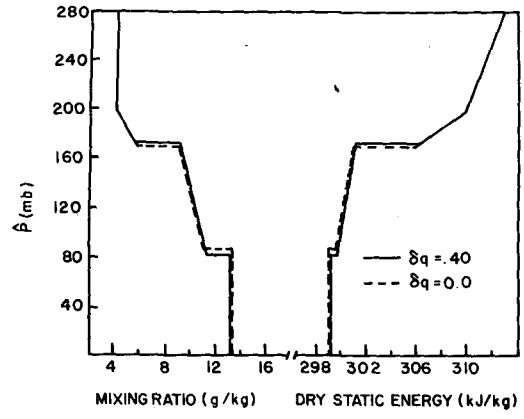

FIG. 7. As in Fig. 4 except for $\delta q = 0.4$ and 0.0 g kg^{-1}.

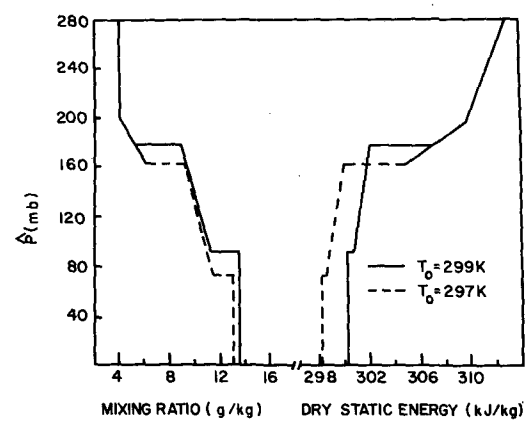

FIG. 9. As in Fig. 4 except for sea surface temperatures of 297 and 299 K.

subsidence warming. Since the subsidence increases slightly with height and the convective cooling and moistening do not vary significantly with divergence, the level at which the balanced described above will occur decreases as the large-scale divergence increases. Although the structure below the inversion does not vary significantly with divergence, the small variations in the depth of the subcloud layer are consistent with the small variations in the subcloud layer values of q and s.

Steady-state solutions obtained with sea surface temperatures of 299 and 297 K are shown in Fig. 9. The principal differences in the structure for these two cases are in the depth of the subcloud layer and in the vertical profile of dry static energy. The dry static energy profile obtained with a sea surface temperature of 297 K is ~2 kJ kg^{-1} less than that obtained with a sea surface temperature of 299 K. The cooler sea surface results in a moisture profile that is ~0.5 g kg^{-1} drier in both the cloud and subcloud layer. It should be noted that while the cooler sea surface temperature results in a lower trade inversion, the cloud base is lower by an approximately equivalent amount. Consequently, the model predicts that the depth of the cloud layer does not depend significantly on the sea surface temperature. In comparison, the results given in Fig. 8 indicate that the depth of the subcloud layer is nearly independent of the large-scale divergence while the depth of the cloud layer increases with smaller divergence values.

The steady-state model solutions are shown in Fig. 10 for surface wind speeds of 5 and 10 m s^{-1}. This is also equivalent to varying the bulk transfer coefficients C_T and C_q. The profiles shown in Fig. 10 indicate significant variations, particularly in the subcloud layer in both the temperature and moisture structure with variations in the surface wind speed. The structure obtained with a surface wind speed of 5 m s^{-1} indicates a significantly cooler and drier boundary layer than that obtained with $V_0 = 10$ m s^{-1}. The smaller surface wind results in a deeper subcloud layer but a shallower cloud layer.

Surface fluxes of latent and sensible heat corresponding to the steady-state results given in Figs. 9 and 10 are shown in Table 5. For steady-state results the sensible heat flux tends to be small and in some situations negative. In fact, the latent heat flux is the dominant component of the virtual dry static energy flux at the surface. The latent heat flux increases as

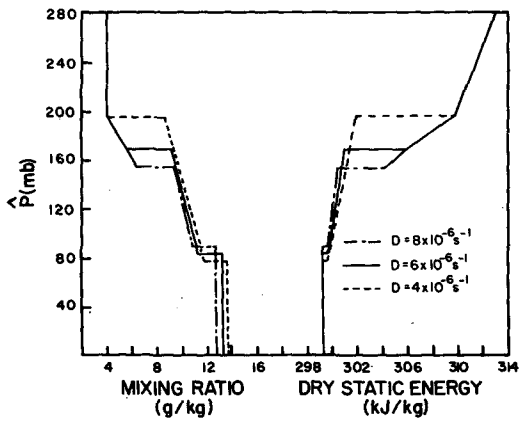

FIG. 8. As in Fig. 4 except for divergence values of 4.0×10^{-6} s^{-1}, 6.0×10^{-6} s^{-1} and 8.0×10^{-6} s^{-1}.

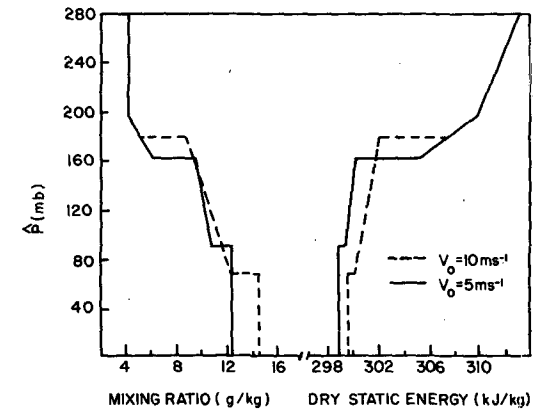

FIG. 10. As in Fig. 4 except for surface wind speeds of 5 and 10 m s^{-1}.

TABLE 5. Depth of the boundary layer and surface fluxes of latent and sensible heat for various sea surface temperatures and wind speeds.

T_0 (K)	V_0 (m s^{-1})	$L(F_q)_0$ (W m^{-2})	$(F_s)_0$ (W m^{-2})	$(F_{sv})_0$ (W m^{-2})	$\hat{p}$ (mb)
297	7	133	1.4	10.9	163.1
299	7	178	1.2	14.0	179.7
298	5	128	4.8	14.0	162.6
298	10	182	−2.6	10.5	179.9

sea surface temperature increases, while the sensible heat flux shows little dependence on the specification of T_0. This indicates that the air-sea differences in q increase with increasing T_0 while air-sea temperature differences are small and relatively insensitive to sea surface temperatures. The latent heat flux also shows an increase with wind speed while the sensible heat flux shows a decrease.

The inversion height is shown in Table 5 for the steady-state results given in Figs. 9 and 10. It is interesting to note the strong positive correlation between the surface flux of moisture and the inversion height.

The results given in Section 4 indicate that the boundary layer radiative heating rates are somewhat insensitive to temperature and moisture variations within the boundary layer. The cloud cover and moisture distribution above the boundary layer, however, may affect the magnitude of both longwave and shortwave heating rates. Starr (1976), for example, has shown that the boundary layer infrared heating is sensitive to the emissivity of higher level clouds. The radiometersonde measurements made during the Line Island Experiment (Albrecht and Cox, 1975) indicate significant variations in the lower level heating rates due to upper level cloudiness. As indicated previously, there is also some uncertainty in the magnitude of heating by the direct absorption of solar radiation. The effect of variations in the average boundary-layer heating rates was evaluated by varying Q_L. The steady-state model solutions are shown in Fig. 11 for $Q_L=-4$ and -2°C day^{-1}. Since the solar heating rate integrated over the entire day is assumed to be 0.8°C day^{-1}, results shown in Fig. 11 are for radiative heating rates of -3.2 and -1.2°C day^{-1}. These variations in the boundary-layer heating may alternately be interpreted as an increase in the solar absorption. The results shown in Fig. 11 show that the model structure predicted with suppressed longwave cooling is warmer by ~0.5°C than that obtained with $Q_L=-4$°C day^{-1}. The suppressed cooling also results in a more moist but shallower boundary layer. The height of the inversion is ~25 mb lower for $Q_L=-2$°C day^{-1} than it is for $Q_L=-4$°C day^{-1}. Cloud base only differs by ~10 mb for these two cases. Since the large-scale divergence field may also be modulated by the radiative effect of upper level clouds (Albrecht and Cox, 1975), it is apparent that these clouds may significantly affect the boundary-layer structure.

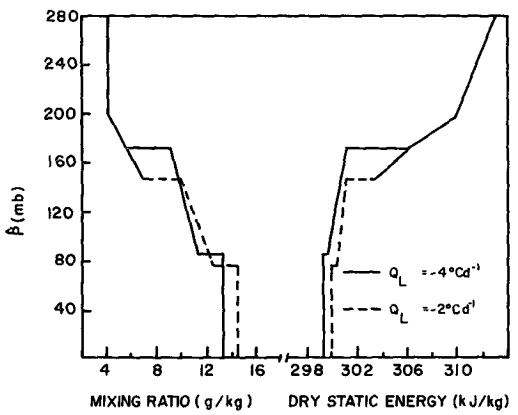

FIG. 11. As in Fig. 4 except for boundary-layer longwave heating rates of −4 and −2°C day^{-1}.

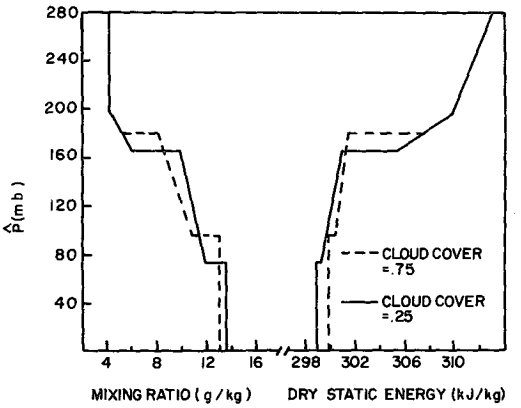

FIG. 12. As in Fig. 4 except for cloud covers of 0.25 and 0.75.

A significant feature of the radiative processes described in Section 4 is the variation in the vertical distribution of the longwave and shortwave heating rates due to variations in the amount of cloud cover. The observations presented by LeMone and Pennell (1976) indicate a significant variation in the amount of boundary-layer cloudiness. They reported cloud covers ranging from 7 to 70% during the aircraft measurements they made to the north of Puerto Rico. The steady-state solutions for visible cloud covers of 0.25 and 0.75 are shown in Fig. 12. The differences in the model structure are not extremely large; however, the effect of cloud-top cooling on varying the height of the inversion is evident. The larger cloud cover results in the trade inversion being approximately 15 mb higher than that obtained with a cloud cover of 0.25. The suppressed cloud- and subcloud-layer heating rates associated with 0.75 cloud cover result in the cloud and subcloud layer being warmer than the structure predicted with a cloud cover of 0.25. The moisture profiles shown in Fig. 12 show a decrease in the cloud layer moisture as the cloud cover is increased. This decrease

in moisture in the cloud layer might actually result in a decrease in visible cloud cover in the real atmosphere. Consequently, the results given in Fig. 12 indicate that the variation in the vertical distribution of the radiative heating due to cloud cover may act as a factor which stabilizes the amount of cloud cover in the real atmosphere. These results indicate that it would be desirable to express cloud cover as a function of the large-scale thermodynamic structure.

6. Conclusions

This paper presents the development and sensitivity testing of a one-dimensional predictive model of the trade-wind boundary layer. The analysis is simplified by assuming that moist static energy and water vapor mixing ratio are constant with pressure in the subcloud layer and linear with pressure in the cloud layer. The subcloud and cloud layers are separated by a transition layer which is assumed to be infinitesimally thin and the upper boundary of the model is defined by the trade inversion which is also assumed to be infinitesimally thin. Heat and moisture budgets are used to derive equations which express the time variation of this simplified structure in terms of the large-scale subsidence (a specified parameter) and convective and radiative fluxes. These equations may be integrated numerically provided the convective and radiative fluxes are defined in terms of the boundary-layer structure itself.

The surface fluxes of heat and moisture are given by a bulk aerodynamic formulation while fluxes at the top of the subcloud layer are specified with a mixed-layer parameterization. The cloud-layer fluxes are represented as the product of a mass flux term which is linear with pressure and a cloud-environment difference in thermodynamic quantities which is linear with pressure. Closure is obtained by assuming that cloud base is at the transition layer, the cloud-environment difference in virtual temperature averaged over the depth of the cloud layer is a constant ΔT_0, and by assuming an adjustment time τ_a that is constant. The numerical results indicate that the model structure is relatively insensitive to the specification of ΔT_0 or τ_a.

Radiative transfer calculations were performed and show that the average radiative heating in the cloud layer is relatively insensitive to variations in temperature, moisture and cloud cover within the boundary layer. The vertical distribution of the radiative heating does, however, vary significantly with the amount of boundary layer cloudiness. In the clear atmosphere the longwave cooling and shortwave heating are nearly uniformly distributed within the boundary layer. In clouds, however, the heating and cooling are confined to a thin layer at cloud top. This cloud-top radiative heating and cooling is explicitly included in the budget equations used to predict the height of the inversion in the model.

The sensitivity of the predicted structure to variations in various physical parameters of the model was shown to be physically plausible. The thermodynamic structure below the inversion was shown to be sensitive to the specification of sea surface temperature, surface wind speed, radiative heating and cloud cover. The height of the inversion was shown to be sensitive to these parameters and the specification of the large-scale divergence.

The results presented in this paper indicate that the model developed may be a useful tool for investigating various aspects of the undisturbed oceanic boundary layer. Some applications of the model are considered in Part II.

Acknowledgments. This research has been supported by the Global Atmospheric Research Program, National Science Foundation, and the GATE Project Office, NOAA, under Grants OCD-74-21678, ATM-77-15369 and ATM-76-09370.

APPENDIX

Computational Details

Numerical results from the model are obtained by integrating the predictive equations described in Section 2 using a Runge-Kutta fourth-order scheme. A summary of the model unknowns is given in Table 3. In this appendix a computational scheme for obtaining these unknowns is described.

The differential equations used to predict h_M and q_M are (5) and (6), while the mixed-layer depth is predicted using (13) or (14). The average value of h and q in the cloud layer is predicted using (7) and (8) and the slopes of these quantities in the cloud layer are predicted using (11) and (12). The height of the trade inversion is predicted using (15) or (16).

To evaluate the time derivative for each of these equations it is necessary to evaluate the convective and radiative fluxes at various levels within the boundary layer. The order in which the fluxes are calculated is important since some fluxes are expressed in terms of others.

To calculate the fluxes, the surface fluxes are calculated first using (17) and (18) so that (23) and (24) may be used to evaluate the fluxes just below the transition layer. In order to calculate the fluxes just above the transition layer it is necessary to calculate $\tilde{\omega}_B$ from (33). The functions f_1 and f_2 which appear in (33) may be evaluated using the definition of mixing ratio and Teton's formula (see A77) so that

$$f_1=\frac{(p_0-\hat{p}_B)}{(T^*-\kappa T_B)s_M}, \tag{A1}$$

$$f_2=\frac{T^*(p_0-\hat{p}_B-e_s)}{(T^*-\kappa T_B)(q_M+\delta q)}, \tag{A2}$$

where T_B is the temperature at the base of the transition layer, e_s is the saturation vapor pressure at the temperature T_B, $T^*=(T_B+\delta T-35.86)^2/4098$, and $\kappa=0.287$. The quantity $\bar{\omega}_B$ may then be determined from (32), (A1), (A2), (5) and (6). The fluxes just above the transition layer may be evaluated from (33) and (34) and ω_B^* calculated from (35).

To evaluate the convective fluxes in the cloud layer it is necessary to determine the entrainment factor E. This parameter is evaluated by applying the constraint given by (40). The exact form of this constraint may be obtained by noting that if the effect of liquid water is considered, the cloud-environment difference of virtual dry static energy may be written

$$s_{vc}-s_v=(s_c-s)+\delta\epsilon L(q_c-q)-\epsilon Ll_c, \tag{A3}$$

where $\epsilon=c_p\bar{T}/L$ and $\delta=0.608$. It is convenient to write (43) as

$$s_{vc}-s_v=\beta(h_c-h)-\epsilon L(q_c+l_c-q)-\alpha L(q^*-q), \tag{A4}$$

where

$$\beta=\frac{1+\gamma\epsilon(1+\delta)}{1+\gamma},\quad \alpha=\frac{1-\epsilon(1+\delta)}{1+\gamma}, \tag{A5}$$

and q^* is the saturation mixing ratio of the environment. The quantity γ which appears in the expression for α and β is

$$\gamma\equiv\frac{L}{c_P}\left(\frac{\partial q^*}{\partial T}\right)_{\hat{p}}. \tag{A6}$$

For the calculations presented in this paper it is assumed that ϵ, α and β are constant with values of $\epsilon=0.12$, $\alpha=0.31$ and $\beta=0.50$.

It is convenient to approximate q^* as a linear function of $\hat{p}$ so that

$$q^*=q_B^*+\gamma_{q^*}(\hat{p}-\hat{p}_B), \tag{A7}$$

where q_B^* is the saturation mixing ratio at cloud base and γ_{q^*} the slope of q^* (see A77). Eqs. (A7), (27) and (28) may then be combined with (A4) to obtain

$$\begin{aligned}s_{vc}-s_v=&-\beta(\Delta h)_{CB}(1+\lambda_h p')+\epsilon L(\Delta q)_{CB}(1+\lambda_q p')\\&-\alpha L[q_B^*-q_{B+}+(\gamma_q^*-\gamma_q)p'],\end{aligned} \tag{A8}$$

where λ_h and λ_q are defined by (38) and (39). With α and β constant, (A8) may be substituted into (40) and integrated. Since λ_h and λ_q depend only on E the above operation results in an expression which when solved for E gives

$$E=[-b-(b^2-4ac)^{\frac{1}{2}}]/2a, \tag{A9}$$

where

$$\begin{aligned}a&=[-\beta(\Delta h)_{CB}+\epsilon L(\Delta q)_{CB}]/3,\\b&=-3a+(\beta\delta\hat{p}\gamma_h-\epsilon L\delta\hat{p}\gamma_q)/3,\\c&=-\beta\delta\hat{p}\gamma_h+\epsilon L\delta\hat{p}\gamma_q-\alpha L\delta\hat{p}(\gamma_q^*-\gamma_q)\\&\quad-2[\beta(\Delta h)_{CB}-\epsilon L(\Delta q)_{CB}+\alpha L(q_B^*-q_B)+c_p\Delta T_0].\end{aligned}$$

The dependence of E on the large-scale stability may be demonstrated more clearly by neglecting virtual temperature effects, ignoring the negative buoyancy at cloud base, and neglecting the $-E/3$ term in the expressions for λ_h and λ_q. With these approximations it may be shown that (40) gives

$$E=\frac{\delta\hat{p}\gamma_{h^*}}{(\Delta h)_{CB}}+\frac{2(1+\gamma)c_p\Delta T_0}{(\Delta h)_{CB}}, \tag{A10}$$

where γ_{h^*} is the slope of moist static energy $h^*=c_pT+gz+Lq^*$ in the cloud layer. As the cloud layer becomes more stable γ_{h^*} becomes less negative which results in E decreasing since $(\Delta h)_{CB}$ is less than zero. Likewise for a given stratification a larger ΔT_0 results in a smaller E.

In situations where the cloud layer is very stable or where the cloud layer is shallow, it is possible that (A9) can result in small and possibly negative entrainment rates. This situation is not permitted by assuming that if $E<0.1$ than $E=0.1$ provided that

$$\int_0^{\hat{p}_I}(F_{sv})d\hat{p}\gtrsim 0. \tag{A11}$$

The factor E is used to define λ_h, λ_q and μ [Eqs. (38), (39) and (42)]. These parameters may then be combined with ω_B^* and $(\Delta h)_{CB}$ and $(\Delta q)_{CB}$ in Eqs. (27) and (28) to define the cloud layer fluxes. The fluxes at $\hat{p}=\hat{p}_A$ are simply obtained by evaluating (27) and (28) at that level.

A slight complication exists in the specification of the fluxes at the top of the cloud layer. This complication arises from the constraint that the inversion is infinitesimally thin and assumed to be at the same height in the temperature and moisture field. In the real atmosphere, the height and/or thickness of the inversion in the temperature profile may differ slightly from that in the moisture field. However, if the inversion in the temperature and moisture field is to remain at the same level in the model, the predictive equations for the height of the inversion (15) and (16) imply that

$$\frac{(F_h)_{I-}-\Delta F_R}{(\Delta h)_I}=\frac{(F_{q+l})_{I-}}{(\Delta q)_I}, \tag{A10a}$$

or alternately

$$\frac{(F_{sl})_{I-}-\Delta F_R}{(\Delta s)_I}=\frac{(F_{q+l})_{I-}}{(\Delta q)_I}, \tag{A10b}$$

where $\Delta F_R=(F_R)_{I+}-(F_R)_{I-}$ and $F_{sl}=F_s-LF_l=F_h-LF_{q+l}$. A similar consistency relationship is considered in the stratocumulus model described by Lilly (1968) and Schubert (1976). The fluxes given by (27) and (28), however, do not satisfy (A10) by definition. In order to insure that (A10) is satisfied it is assumed that

$$(F_h)_{I-}=(F_h)^{\text{conv}}+L(F_{q+l})_{I-}^{\text{res}}, \tag{A11a}$$

$$(F_{q+l})_{I-}=(F_{q+l})_{I-}^{\text{conv}}+(F_{q+l})_{I-}^{\text{res}}, \tag{A11b}$$

$$(F_{sl})_{I-}=(F_h)_I^{\text{conv}}-L(F_{q+l})_{I-}^{\text{conv}}, \tag{A11c}$$

where $(F_h)_{I-}^{conv}$ and $(F_{q+l})_{I-}^{conv}$ are the convective fluxes given by (27) and (28) and $(F_{q+l})_{I-}^{res}$ is a residual flux that is introduced to allow the inversion height to be predicted consistently for the moisture and the temperature variables. This residual flux is evaluated by substituting (A11) into (A10) and solving for $(F_{q+l})_{I-}^{res}$. This procedure gives

$$(F_{q+l})_{I-}^{res}=\left\{\frac{\dfrac{(\Delta h)_I}{(\Delta q)_I}(F_{q+l})_{I-}^{conv}-(F_h)_{I-}^{conv}+\Delta F_R}{1-\dfrac{(\Delta h)_I}{L(\Delta q)_I}}\right\}. \quad \text{(A12)}$$

The assumption made in (A11) is equivalent to predicting the inversion height with the expression

$$\frac{\partial \hat{p}_I}{\partial t}=\hat{\omega}_I-g\frac{[(F_{sl})_{I-}-\Delta F_R]}{(\Delta s)_I}, \quad \text{(A13)}$$

where $(F_{sl})_{I-}=(F_h)_{I-}^{conv}-L(F_{q+l})_{I-}^{conv}$. Note that the residual flux does not appear in (A13). Physically this computational procedure implies that the temperature profile determines the height of the inversion. If the height of the moisture discontinuity as predicted by simply using the convective fluxes in (16) differs slightly from the predicted height in the temperature profile, the moisture profile adjusts to the temperature profile. The flux required for this adjustment is simply $(F_{q+l})_{I-}^{res}$ which allows the height of the moisture discontinuity to adjust at the expense of the cloud-layer moisture. If this flux was not introduced [i.e., using (A13) to predict the height of the inversion and $(F_h)_{I-}^{conv}$ and $(F_{q+l})_{I-}^{conv}$ in the cloud-layer budget equations] moisture could be fictitiously lost or gained from the model. In actual calculations it is found that the residual flux is small compared to $(F_{q+l})_{I-}^{conv}$.

The radiative fluxes in the model are calculated from (47)–(50). It is necessary to calculate the fluxes by the procedure outlined above at each point where it is necessary to evaluate the time derivative. For the Runge-Kutta procedure it is necessary to evaluate the derivatives four times at each time step. All the results presented in this paper were obtained using a time step of 12 min. Runs made using shorter time steps resulted in nearly identical solutions. An integration over one hour of model time requires approximately 0.6 s of CDC 6400 time.

REFERENCES

Albrecht, B. A., 1977: A time-dependent model of the trade-wind boundary layer. Ph.D. dissertation, Colorado State University, 174 pp.

——, 1979: A model of the thermodynamic structure of the trade-wind boundary layer: Part II. Applications. *J. Atmos. Sci.*, **36**, 111–111.

——, and S. K. Cox, 1975: The large-scale response of the tropical atmosphere to cloud modulated infrared heating. *J. Atmos. Sci.*, **32**, 16–24.

Arakawa, A., and W. H. Schubert, 1974: Interaction of a cumulus cloud ensemble with the large-scale environment, Part I. *J. Atmos. Sci.*, **31**, 674–701.

Augstein, A., H. Schmidt and F. Ostapoff, 1974: The vertical structure of the atmospheric planetary boundary layer in undisturbed trade winds over the Atlantic ocean. *Bound.-Layer Meteor.*, **6**, 129–150.

——, H. Riehl, F. Ostapoff and V. Wagner, 1973: Mass and energy transports in an undisturbed Atlantic trade wind flow. *Mon. Wea. Rev.*, **101**, 101–111.

Betts, A. K., 1973: Non-precipitating cumulus convection and its parameterization. *Quart. J. Roy. Meteor. Soc.*, **86**, 178–196.

——, 1975: Parametric interpretation of trade-wind cumulus budget studies. *J. Atmos. Sci.*, **32**, 1934–1945.

——, 1976a: Modeling subcloud layer structure and interaction with a shallow cumulus layer. *J. Atmos. Sci.*, **33**, 2363–2382.

——, 1976b: The thermodynamic transformation of the tropical subcloud layer by precipitation downdrafts. *J. Atmos. Sci.*, **33**, 1008–1020.

Bunker, A. F., B. Haurwitz, J. S. Malkus and H. Stommel, 1949: Vertical distribution of temperature and humidity over the Caribbean sea. *Pap Phys. Oceanogr. Meteor.*, **11**, 82 pp.

Cox, S. K., 1973: Infrared heating calculations with a water vapor pressure broadened continuum. *Quart. J. Roy. Meteor. Soc.*, **99**, 669–679.

Deardorff, J. W., 1972: Numerical investigations of neutral and unstable boundary layers. *J. Atmos. Sci.*, **29**, 91–115.

Esbensen, S., 1975: An analysis of the subcloud layer heat and moisture budgets in the western Atlantic trades. *J. Atmos. Sci.*, **32**, 1921–1933.

——, 1976: Thermodynamic effects of clouds in the trade wind planetary boundary layer. Ph.D. thesis, UCLA, 110 pp.

Feigel'son, E. M., 1973: *Radiant Heat Transfer in a Cloudy Atmosphere.* Israel Program for Scientific Translations, Jerusalem, 191 pp.

Fissel, D. B., S. Pond and M. Miyake, 1977: Computation of surface fluxes from climatological and synoptic data. *Mon. Wea. Rev.*, **105**, 26–36.

Fraedrich, K., 1973: On the parameterization of cumulus convection by lateral mixing and compensating subsidence, Part I. *J. Atmos. Sci.*, **30**, 408–413.

——, 1976: A mass budget of an ensemble of transient clouds determined from direct cloud observations. *J. Atmos. Sci.*, **33**, 262–268.

Friehe, C. A., and K. F. Schmitt, 1976: Parameterization of air sea interface fluxes of sensible heat and moisture by the bulk aerodynamic formulas. *J. Phys. Oceanogr.*, **6**, 801–809.

Griffith, K. T., and S. K. Cox, 1977: Infrared properties of tropical cirrus clouds inferred from broadband measurements. Atmos. Sci. Pap. No. 269, Colorado State University, 102 pp. [NTIS No. PB-268531.]

Holland, J., and E. Rasmusson, 1973: Measurements of the atmospheric mass, energy, and momentum budgets over a 500-kilometer square of tropical ocean. *Mon. Wea. Rev.*, **101**, 44–55.

Kuo, H. L., 1965: On the formation and intensification of tropical cyclones through latent heat release by cumulus convection. *J. Atmos. Sci.*, **22**, 40–63.

——, 1974: Further studies of the parameterization of the influence of cumulus convection on large-scale flow. *J. Atmos. Sci.*, **31**, 1232–1240.

LeMone, M. A., and W. T. Pennell, 1976: The relationship of trade wind cumulus distribution to subcloud layer fluxes and structure. *Mon. Wea. Rev.*, **104**, 524–539.

Lilly, D. K., 1968: Models of cloud-topped mixed layers under a strong inversion, *Quart. J. Roy. Meteor. Soc.*, **94**, 292–309.

Liou, K-N., 1976: On the absorption, reflection and transmission of solar radiation in cloudy atmospheres. *J. Atmos. Sci.*, **33**, 798–505.

Malkus, J. S., 1958: On the structure of the trade wind moist layer. *Pap. Phys. Oceanogr. Meteor.*, **12**, No. 2, 47 pp.

Manabe, S., and F. Moller, 1961: On the radiative equilibrium and heat balance of the atmosphere. *Mon. Wea. Rev.*, **89**, 503–532.

Nitta, T., 1975: Observational determination of cloud mass flux distributions. *J. Atmos. Sci.*, **32**, 73–91.

——, and S. Esbensen, 1974: Heat and moisture budgets using BOMEX data. *Mon. Wea. Rev.*, **102**, 17–28.

Ogura, Y., and H-R Cho, 1974: On the interaction between the subcloud and cloud layers on tropical regions. *J. Atmos. Sci.*, **31**, 1850–1859.

——, M. H. Russel and H-R Cho, 1977: A semi-empirical model of the trade-wind inversion. *J. Meteor. Soc. Japan*, **55**, 209–220.

Ooyama, K., 1971: A theory on parameterization of cumulus convection. *J. Meteor. Soc. Japan*, **49** (Special issue), 744–756.

Paltridge, G. W., 1974: Infrared emmissivity, short-wave albedo, and the microphysics of stratiform water clouds. *J. Geophys. Res.*, **79**, 4053–4058.

Reynolds, D. W., T. H. Vonder Haar and S. K. Cox, 1975: The effect of solar radiation absorption in the tropical troposphere. *J. Appl. Meteor.*, **14**, 433–444.

Riehl, H., and J. S. Malkus, 1957: On the heat balance and maintenance of circulation in the trades. *Quart. J. Roy. Meteor. Soc.*, **83**, 21–28.

——, T. C. Yeh, J. S. Malkus and N. E. LeSeur, 1951: The northeast trade of the Pacific ocean. *Quart. J. Roy. Meteor. Soc.*, **72**, 598–626.

Sarachik, E. S., 1974: The tropical mixed layer and cumulus parameterization. *J. Atmos. Sci.*, **31**, 2225–2230.

Schubert, W. H., 1976: Experiments with Lilly's cloud-topped mixed layer model. *J. Atmos. Sci.*, **33**, 436–446.

Seguin, W. R., and M. Garstang, 1976: Some evidence of the effects of convection on the structure of the tropical subcloud layer. *J. Atmos. Sci.*, **33**, 660–666.

Sommeria, G., 1976: Three dimensional simulation of turbulent processes in the undisturbed trade wind boundary layer. *J. Atmos. Sci.*, **33**, 216–241.

Starr, D. O'C., 1976: The sensitivity of tropical radiative budgets to cloud distribution and the radiative properties of clouds. Atmos. Sci. Pap. No. 254, Colorado State University, 117 pp. [NTIS No. PB-263227.]

Stull, R. B., 1976a: Mixed-layer depth model based on turbulent energetics. *J. Atmos. Sci.*, **33**, 1268–1278.

——, 1976b: The energetics of entrainment across a density interface. *J. Atmos. Sci.*, **33**, 1260–1267.

Tennekes, H., 1973: A model for the dynamics of the inversion above a convective boundary layer. *J. Atmos. Sci.*, **30**, 558–567.

Twomey, S., 1976: Computations of the absorption of solar radiation by clouds. *J. Atmos. Sci.*, **33**, 1087–1091.

Yanai, M., S. Esbensen and J. H. Chu, 1973: Determination of bulk properties of tropical cloud clusters from large-scale heat and moisture budgets. *J. Atmos. Sci.*, **30**, 611–627.

Zeman, O., and H. Tennekes, 1977: Parameterization of the turbulent energy budget at the top of the daytime atmospheric boundary layer. *J. Atmos. Sci.*, **34**, 111–123.